

## A Non-orthogonal Primitive Equation Coastal Ocean Circulation Model: Application to Lake Superior

Changsheng Chen<sup>1,\*</sup>, Jianrong Zhu<sup>2</sup>, Lianyuan Zheng<sup>3</sup>, Elise Ralph<sup>4</sup>, and Judith Wells Budd<sup>5</sup>

<sup>1</sup>*School of Marine Science and Technology  
University of Massachusetts-Dartmouth  
New Bedford, Massachusetts 02742*

<sup>2</sup>*State Key Laboratory of Estuarine and Coastal Research  
East China Normal University  
Shanghai 200062, P. R. China*

<sup>3</sup>*College of Marine Science  
University of South Florida  
St. Petersburg, Florida 33701*

<sup>4</sup>*The Large Lakes Observatory  
University of Minnesota  
Duluth, Minnesota 55812*

<sup>5</sup>*Department of Geological Engineering and Sciences  
Michigan Technological University  
Houghton, Michigan 49931*

**ABSTRACT.** A non-orthogonal coordinate primitive equation model has been developed for the study of the Keweenaw Current in Lake Superior. This model provides a more accurate fitting of the coastline. A comparison with a curvilinear orthogonal model shows that the non-orthogonal transformation model provided a better simulation of the current jet in the near-shore region. Accurate fitting of both bathymetry and irregular coastlines plays an essential role in capturing the magnitude of the Keweenaw Current and cross-shelf structure of the thermal bar near the coast. The formation of the Keweenaw Current and thermal front was directly driven by a westerly or southwesterly wind and seasonal development of stratification over steep bottom topography. Under a condition with accurate fitting of steep bathymetry, failure to resolve the irregular geometry of the coastline can result in an underestimation of the magnitude of the Keweenaw Current by about 20 cm/s.

**INDEX WORDS:** Numerical modeling, thermal bar, Keweenaw Current, Lake Superior, numerical methods.

### INTRODUCTION

Lake Superior, one of the largest lakes in the world, has an east-west length of about 600 km and a south-north width of 250 km. It has a coastline of about 5,000 km, with a narrow “continental shelf” of about 10–15 km around the coast. The average slope of the shelf is about 0.01 on the northern coast, about 0.05 on the western and eastern coasts,

and 0.035 on the southern coast. The steepest slope of the shelf, exceeding 0.05, occurs along the Keweenaw Peninsula (Fig. 1). In the interior, the mean depth is about 150 m, but the maximum depth is greater than 400 m.

The circulation in Lake Superior is driven mainly by winds and buoyancy (Jacobs 1974, Bennett 1978, Chen *et al.* 2001, Zhu *et al.* 2001). Currents vary significantly with seasons. They are weak and reverse intermittently in spring and fall due to frequent changes of the wind’s direction under the

\*Corresponding author. E-mail: c1chen@umassd.edu

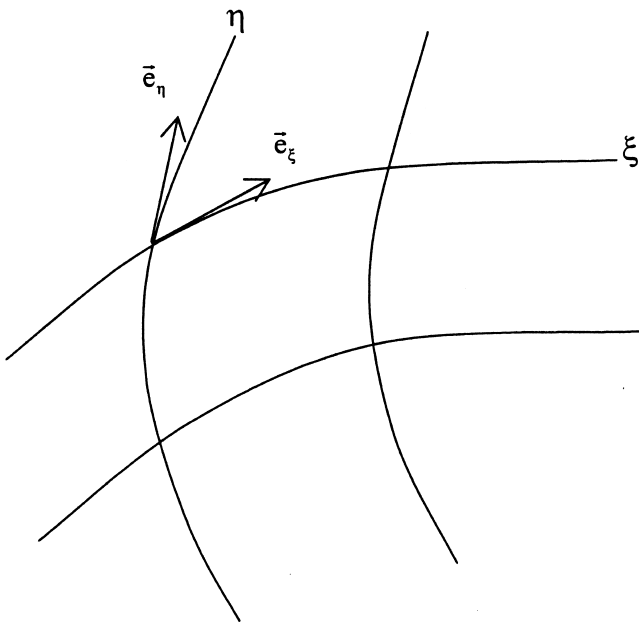


**FIG. 1. Bathymetry of Lake Superior (a) and moored buoy sites (b). Solid circles are the locations of moored current meter labeled 1, 2 and 3. The unit of the bathymetry is meters.**

condition of weak stratification. During summer, currents are stronger and relatively stable, as a result of the dominance of the northeastward wind plus the formation and intensification of coastal thermal front (Hubbard and Spain 1973, Spain *et al.* 1976). A northeastward coastal current (called the Keweenaw Current) is a nearly permanent feature along the Keweenaw coast in summer, forming a major characteristic of the circulation in Lake Superior (Ragotzkie 1966, Smith and Ragotzkie 1977, Niebauer *et al.* 1977, Phillips 1978, Viekman and Wimbush 1993). The Keweenaw Current is confined within a narrow near-shore band of order 5-km in width. It is affected significantly by the inner shelf physical processes associated with wind mixing, and wind-induced convergence (downwelling) and divergence (upwelling) near the coast.

One of the objectives of the Keweenaw Interdisciplinary Transport Experiment in Superior Lake (KITES) is to determine the effects of physical, chemical, and biological processes that arise from the formation, evolution, and perturbation of the thermal bar and Keweenaw Current on the distinct nearshore and offshore ecosystems in Lake Superior. Since these processes are nonlinearly coupled with each other, it is difficult to examine, verify,

and understand the ecosystem dynamics merely through observations taken either at a given time or at a few monitoring stations. Developing a validated full three-dimensional, prognostic numerical model will provide us with a scientific tool to examine these complex environmental problems.

In the last 30 years, many efforts have been made on developing the Lake Superior model. Lam (1978) was a first person who developed a four-layer model. Driven by realistic wind and buoyancy forcing, his model did produce a current jet along the Keweenaw coast, but the model-predicted speed was only about 5 to 7 cm s<sup>-1</sup>, that is, 5 to 10 times smaller than that observed by Niebauer *et al.* (1977). The cases for this underestimation were believed due to (1) the low cross-shelf model resolution, (2) the lack of surface heating, and (3) the failure to resolve irregular coastal geometry (Chen *et al.* 2001; Zhu *et al.* 2001). A uniform horizontal resolution of 10 km was used in Lam's (1978) model experiment. This numerical resolution was larger than the general cross-shelf scale of the Keweenaw Current observed in summer. The model computational domain was configured with structured rectangular grid meshes. These meshes poorly matched the shape of the coastline along the Keweenaw Peninsula. The step-like boundary constructed from these rectangular meshes causes artificial drag force to slow down the along-coast current.

Chen *et al.* (2001) developed a so-called non-orthogonal coordinate transformation oceanic model for Lake Superior. The non-orthogonal coordinate transformation allows us to make numerical meshes more flexible in shapes by removing the requirement of a strict orthogonal (90°) condition of mesh angles. The model with the non-orthogonal coordinate transformation provides a better fitting of irregular coastline, which is believed to play a critical role in the simulation of the near-shore current jet. This new model has successfully simulated the currents and thermal front (in the Great Lakes community, it is called "thermal bar") observed along the Keweenaw coast in Lake Superior (Chen *et al.* 2001, Zhu *et al.* 2001). The model-predicted water transport has been used to guide the process studies of the impact of physical processes on the temporal and spatial distributions of the biological variables observed during the KITE field measurements.

One of the critical fundamental technical issues was raised on the non-orthogonal coordination transformation model: Do we really need such a

model to be successful in simulating the water current and transport in Lake Superior? The curvilinear orthogonal coordinate transformation model, which requires all angles of individual numerical mesh to satisfy  $90^\circ$ , has been widely used in the Great Lakes community. These models provide a moderate fit for the irregular coastal boundary. However, because this method requires a strict orthogonal ( $90^\circ$ ) condition, a grid generation program using a fast Poisson solver of the Laplace equation makes reaching a convergence solution difficult and also fails to fit an irregular coastline characterized with complex geometric boundary (like one shown in Keweenaw Peninsula). Applying this transformation to the coast with a concave bend usually results in a poor resolution near the coast.

The limitation of a curvilinear orthogonal coordinate transformation model in application to coastal regions has been recognized for many years in the coastal ocean community. The successful application of the non-orthogonal coordinate transformation model to Lake Superior indirectly implies the importance of the geometric fitting in that area. Since no quantitative comparisons between orthogonal and non-orthogonal coordinate transformation models have been made regarding the realistic simulation, the accuracy of the non-orthogonal coordinate transformation oceanic model is still not validated.

The objective of this study is to provide a quantitative validation of the importance of coastal geometric fitting in simulating the Keweenaw Current in Lake Superior. To achieve this goal, we re-ran the simulation using both curvilinear orthogonal and non-orthogonal coordinate transformation versions of ECOM-si (Blumberg 1994) and compared the model results with the observed currents at three buoy sites off Eagle Harbor along the Keweenaw coast. A sensitivity study clearly shows that the non-orthogonal transformation model provides a better simulation of the current in the near-shore region. Accurate fitting of bathymetry and irregular coastlines plays an essential role in capturing the magnitude of the Keweenaw Current and cross-shelf structure of the thermal front near the coast. The formation of the Keweenaw Current and thermal front was directly driven by the westerly or southwesterly wind and seasonal development of stratification over steep bottom topography. Under a condition with accurate fitting of steep bathymetry, failure to resolve the irregular geometry of the coastline can result in an underestimation of the

magnitude of the Keweenaw Current by about 20 cm/s.

The remaining sections are organized as follows. The non-orthogonal model formulation section describes the primitive equation of the coastal model with a non-orthogonal coordinate transformation. The numerical computational method section represents the numerical methods used to solve the model. The model application and validation section shows examples of the application of this model to Lake Superior. Finally, the conclusion is given in the last section.

## THE NON-ORTHOGONAL MODEL FORMULATION

### The Primitive Equations

The governing equations of ocean circulation and water masses consist of momentum, continuity, temperature, salinity, and density equations as follows:

$$\frac{\partial u}{\partial t} + u \frac{\partial u}{\partial x} + v \frac{\partial u}{\partial y} + w \frac{\partial u}{\partial z} - fv = -g \frac{\partial \zeta}{\partial x} - \frac{\partial P}{\partial x} + \frac{\partial}{\partial z} \left( K_m \frac{\partial u}{\partial z} \right) + F_u \quad (1)$$

$$\frac{\partial v}{\partial t} + u \frac{\partial v}{\partial x} + v \frac{\partial v}{\partial y} + w \frac{\partial v}{\partial z} + fu = -g \frac{\partial \zeta}{\partial y} - \frac{\partial P}{\partial y} + \frac{\partial}{\partial z} \left( K_m \frac{\partial v}{\partial z} \right) + F_v \quad (2)$$

$$\frac{\partial u}{\partial x} + \frac{\partial v}{\partial y} + \frac{\partial w}{\partial z} = 0 \quad (3)$$

$$\frac{\partial \theta}{\partial t} + u \frac{\partial \theta}{\partial x} + v \frac{\partial \theta}{\partial y} + w \frac{\partial \theta}{\partial z} = \frac{\partial}{\partial z} \left( K_h \frac{\partial \theta}{\partial z} \right) + \frac{\partial SW}{\partial z} + F_\theta \quad (4)$$

$$\frac{\partial s}{\partial t} + u \frac{\partial s}{\partial x} + v \frac{\partial s}{\partial y} + w \frac{\partial s}{\partial z} = \frac{\partial}{\partial z} \left( K_h \frac{\partial s}{\partial z} \right) + F_s \quad (5)$$

$$\rho_{total} = \rho_{total}(\theta, s) \quad (6)$$

where  $x$ ,  $y$ , and  $z$  are the east, north, and vertical axes of the Cartesian coordinate;  $u$ ,  $v$ , and  $w$  the  $x$ ,  $y$ ,  $z$  velocity components;  $\theta$  the potential temperature;  $s$  the salinity;  $\zeta$  the sea surface elevation;  $P$  the baroclinic pressure defined as  $1/\rho_o \int_z^0 \rho g dz$ ;  $f$  the Coriolis parameter;  $g$  the gravitational acceleration;  $K_m$  the vertical eddy viscosity coefficient;  $K_h$  the thermal vertical eddy diffusion coefficient, and  $SW$  is the

short-wave solar radiation that is a function of  $z$  and  $t$ .  $F_u$ ,  $F_v$ ,  $F_\theta$  and  $F_s$  represent the horizontal momentum, thermal, and salt diffusion terms.  $\rho$  and  $\rho_o$  are the perturbation and reference density, which satisfy

$$\rho_{\text{total}} = \rho + \rho_o. \quad (7)$$

$F_u$ ,  $F_v$ ,  $F_\theta$  and  $F_s$  are calculated by Smagorinsky's formula (Smagorinsky 1963) in which the horizontal diffusion is directly proportional to the product of horizontal grid sizes.  $K_m$  and  $K_h$  are calculated using the Mellor and Yamada (Mellor and Yamada 1974, 1982) level 2.5 turbulent closure scheme, with the modified stability function by Galperin *et al.* (1988). This turbulent-closure model is designed to simulate boundary layer physics through the inclusion of (1) shear and buoyancy production of turbulent kinetic energy, (2) dissipation of turbulent kinetic energy, (3) vertical diffusion and the time derivative of the turbulent kinetic energy and turbulent macroscale, and (4) the advection of the turbulent kinetic energy.

### The Non-Orthogonal Coordinate System

Let us define a new coordinate transformation as

$$\xi = \xi(x, y), \quad \eta = \eta(x, y) \quad (8)$$

Taking the differentiation of Eq. (8) with respect to  $x$  and  $y$ , respectively, yields the interchange relations as

$$\xi_x = \frac{y_\eta}{J}, \quad \xi_y = -\frac{x_\eta}{J}, \quad \eta_x = -\frac{y_\xi}{J}, \quad \eta_y = \frac{x_\xi}{J} \quad (9)$$

where  $J$  is the Jacobian function in the form of

$$J = x_\xi y_\eta - x_\eta y_\xi \quad (10)$$

and the subscript symbols ( $\xi$  and  $\eta$ ) indicate derivatives. The metric factors  $h_1$  and  $h_2$  of the coordinate transformation are defined as

$$h_1 = \sqrt{x_\xi^2 + y_\xi^2}, \quad h_2 = \sqrt{x_\eta^2 + y_\eta^2}. \quad (11)$$

The unit vectors ( $e_\xi$ ,  $e_\eta$ ) for the coordinate ( $\xi, \eta$ ) are defined as

$$e_\xi = \frac{\xi_x i + \xi_y j}{\sqrt{\xi_x^2 + \xi_y^2}}, \quad e_\eta = \frac{\eta_x i + \eta_y j}{\sqrt{\eta_x^2 + \eta_y^2}}, \quad (12)$$

(Fig. 2) and the interchange relation of unit vectors between non-orthogonal ( $\xi, \eta$ ) and orthogonal ( $x, y$ ) coordinates is given by

$$e_\xi = \frac{1}{h_2}(y_\eta i - x_\eta j), \quad e_\eta = \frac{1}{h_1}(-y_\xi i + x_\xi j), \quad (13)$$

Therefore, the  $\xi$  and  $\eta$  components of the velocity (defined as  $u_1, v_1$ ) can be expressed in the form of

$$u_1 = \frac{h_2}{J}(x_\xi u + y_\xi v), \quad v_1 = \frac{h_1}{J}(x_\eta u + y_\eta v). \quad (14)$$

Using this transformation, we can re-write the momentum, continuity, temperature and salinity equations as where

$$\frac{\partial u_1}{\partial t} + \hat{U} \frac{\partial u_1}{\partial \xi} + \hat{V} \frac{\partial u_1}{\partial \eta} + w \frac{\partial u_1}{\partial z} - \frac{h_2 \hat{V}}{J} \left[ v_1 \frac{\partial}{\partial \xi} \left( \frac{J}{h_1} \right) - u_1 \frac{\partial}{\partial \eta} \left( \frac{J}{h_2} \right) + Jf \right] - \quad (15)$$

$$\frac{h_2}{J} u_1 v_1 \frac{\partial}{\partial \xi} \left( \frac{h_3}{h_1 h_2} \right) = -\frac{h_2}{\rho_o J} \frac{\partial P}{\partial \xi} + \frac{\partial}{\partial z} \left( K_m \frac{\partial u_1}{\partial z} \right) + F_x$$

$$\frac{\partial v_1}{\partial t} + \hat{U} \frac{\partial v_1}{\partial \xi} + \hat{V} \frac{\partial v_1}{\partial \eta} + w \frac{\partial v_1}{\partial z} + \frac{h_1 \hat{U}}{J} \left[ v_1 \frac{\partial}{\partial \xi} \left( \frac{J}{h_1} \right) - u_1 \frac{\partial}{\partial \eta} \left( \frac{J}{h_2} \right) + Jf \right] - \quad (16)$$

$$\frac{h_1}{J} u_1 v_1 \frac{\partial}{\partial \eta} \left( \frac{h_3}{h_1 h_2} \right) = -\frac{h_1}{\rho_o J} \frac{\partial P}{\partial \eta} + \frac{\partial}{\partial z} \left( K_m \frac{\partial v_1}{\partial z} \right) + F_y$$

$$\frac{\partial \hat{U}}{\partial \xi} + \frac{\partial \hat{V}}{\partial \eta} + \frac{\partial Jw}{\partial z} = 0 \quad (17)$$

$$\frac{\partial \theta}{\partial t} + \hat{U} \frac{\partial \theta}{\partial \xi} + \hat{V} \frac{\partial \theta}{\partial \eta} + w \frac{\partial \theta}{\partial z} = \frac{\partial}{\partial z} \left( K_h \frac{\partial \theta}{\partial z} \right) + \frac{\partial SW}{\partial z} + F_\theta \quad (18)$$

$$\frac{\partial s}{\partial t} + \hat{U} \frac{\partial s}{\partial \xi} + \hat{V} \frac{\partial s}{\partial \eta} + w \frac{\partial s}{\partial z} = \frac{\partial}{\partial z} \left( K_h \frac{\partial s}{\partial z} \right) + F_s \quad (19)$$

where

$$\hat{U} = \frac{1}{J} \left( h_2 u_1 - \frac{h_3}{h_1} v_1 \right), \quad \hat{V} = \frac{1}{J} \left( h_1 v_1 - \frac{h_3}{h_2} u_1 \right) \quad (20)$$

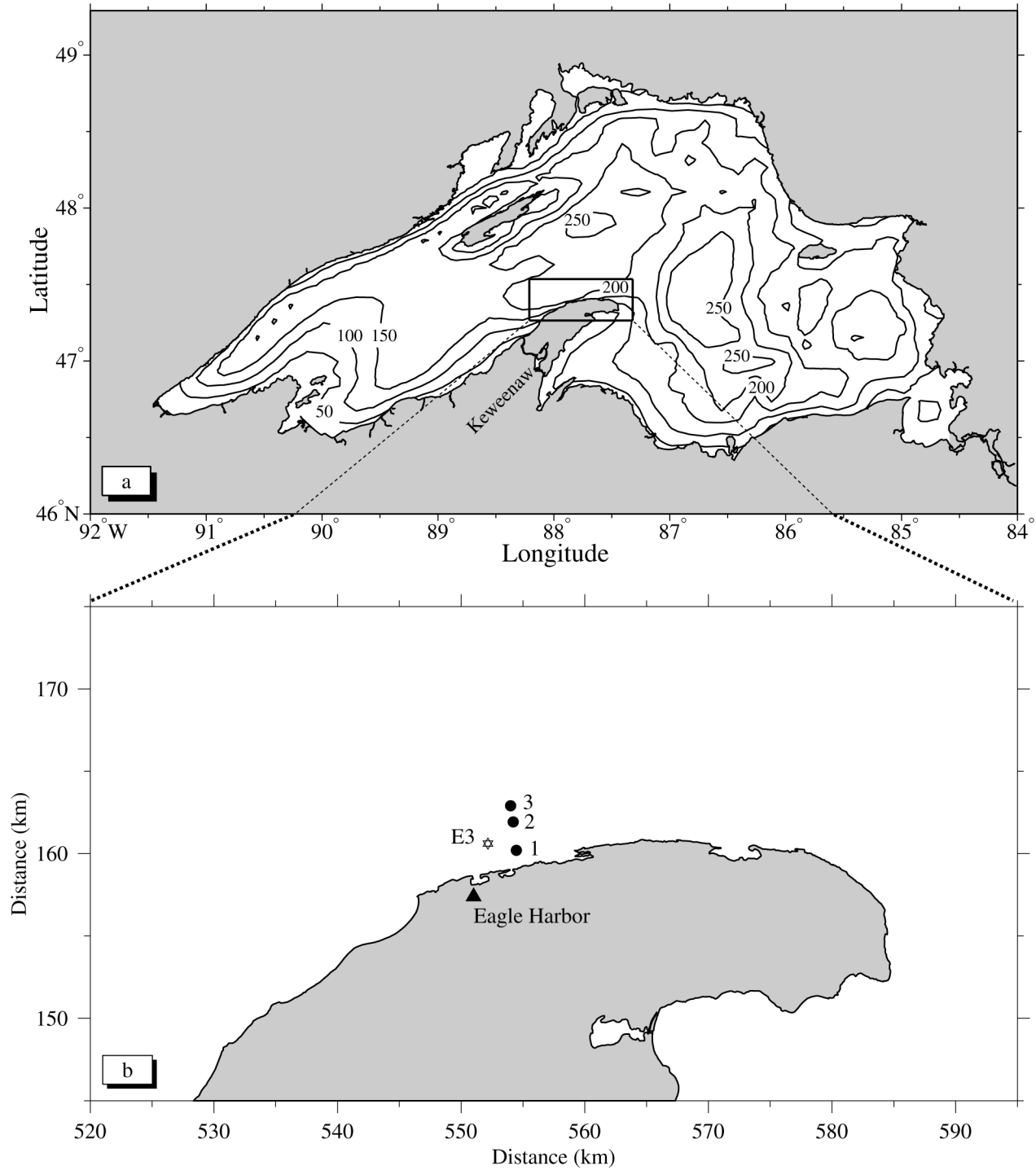


FIG. 2. Illustration of the non-orthogonal coordinate system used in the model.

and

$$h_3 = y_\xi y_\eta + x_\xi x_\eta \quad (21)$$

are the cross-metric factors caused by the non-orthogonal transformation. The non-orthogonal

coordinate transformation used here is completely different from the one introduced in CH3D or CH3D-WES by Sheng (1986) and Chapman et al. (1996). A detailed discussion on the difference is given in Appendix.

### The $\sigma$ -Coordinate Transformation System

To simplify the numerical calculation over an irregular bottom slope, a vertically stretched  $\sigma$ -coordinate transformation is used in the numerical computation. This transformation is defined as

$$\sigma = \frac{z - \zeta}{H + \zeta} \quad (22)$$

where  $H(x, y)$  is the mean water depth and  $D = H + \zeta$ . The vertical coordinate  $\sigma$  varies from  $-1$  at  $z = -H$  to  $0$  at  $z = \zeta$ . In this system, eqs. (15)–(19) can be rewritten with the form of the transport as

$$\begin{aligned} & \frac{\partial DJu_1}{\partial t} + \frac{\partial DJ\hat{U}u_1}{\partial \xi} + \frac{\partial DJ\hat{V}u_1}{\partial \eta} + \frac{\partial J\omega u_1}{\partial \sigma} - \\ & Dh_2\hat{V} \left[ v_1 \frac{\partial}{\partial \xi} \left( \frac{J}{h_1} \right) - u_1 \frac{\partial}{\partial \eta} \left( \frac{J}{h_2} \right) + Jf \right] - Dh_2u_1v_1 \frac{\partial}{\partial \xi} \left( \frac{h_3}{h_1h_2} \right) \\ & = -h_2gD \frac{\partial \zeta}{\partial \xi} + \frac{gh_2D}{\rho_o} \frac{\partial D}{\partial \xi} \int_{\sigma}^0 \sigma \frac{\partial \rho}{\partial \sigma} d\sigma - \frac{gh_2D^2}{\rho_o} \frac{\partial}{\partial \xi} \\ & \int_{\sigma}^0 \rho d\sigma + \frac{1}{D} \frac{\partial}{\partial \sigma} \left( K_m \frac{\partial Ju_1}{\partial \sigma} \right) + DJF_x \end{aligned} \quad (23)$$

$$\begin{aligned} & \frac{\partial DJv_1}{\partial t} + \frac{\partial DJ\hat{U}v_1}{\partial \xi} + \frac{\partial DJ\hat{V}v_1}{\partial \eta} + \frac{\partial J\omega v_1}{\partial \sigma} + \\ & Dh_1\hat{U} \left[ v_1 \frac{\partial}{\partial \xi} \left( \frac{J}{h_1} \right) - u_1 \frac{\partial}{\partial \eta} \left( \frac{J}{h_2} \right) + Jf \right] - Dh_1u_1v_1 \frac{\partial}{\partial \eta} \left( \frac{h_3}{h_1h_2} \right) \\ & = -h_1gD \frac{\partial \zeta}{\partial \eta} + \frac{gh_1D}{\rho_o} \frac{\partial D}{\partial \eta} \int_{\sigma}^0 \sigma \frac{\partial \rho}{\partial \sigma} d\sigma - \frac{gh_1D^2}{\rho_o} \frac{\partial}{\partial \eta} \\ & \int_{\sigma}^0 \rho d\sigma + \frac{1}{D} \frac{\partial}{\partial \sigma} \left( K_m \frac{\partial Jv_1}{\partial \sigma} \right) + DJF_y \end{aligned} \quad (24)$$

$$\frac{\partial \zeta}{\partial t} + \frac{1}{J} \left[ \frac{\partial}{\partial \xi} (DJ\hat{U}) + \frac{\partial}{\partial \eta} (DJ\hat{V}) \right] + \frac{\partial \omega}{\partial \sigma} = 0 \quad (25)$$

$$\begin{aligned} & \frac{\partial JD\theta}{\partial t} + \frac{\partial JD\hat{U}\theta}{\partial \xi} + \frac{\partial JD\hat{V}\theta}{\partial \eta} + \frac{\partial J\omega\theta}{\partial \sigma} = \\ & \frac{1}{D} \frac{\partial}{\partial \sigma} \left( K_h \frac{\partial J\theta}{\partial \sigma} \right) + \frac{\partial SW}{\partial \sigma} + DJF_{\theta} \end{aligned} \quad (26)$$

$$\begin{aligned} & \frac{\partial JDs}{\partial t} + \frac{\partial JD\hat{U}s}{\partial \xi} + \frac{\partial JD\hat{V}s}{\partial \eta} + \frac{\partial J\omega s}{\partial \sigma} = \\ & \frac{1}{D} \frac{\partial}{\partial \sigma} \left( K_h \frac{\partial Js}{\partial \sigma} \right) + DJF_s \end{aligned} \quad (27)$$

where

$$\begin{aligned} \omega = w - \sigma \left( \hat{U} \frac{\partial D}{\partial \xi} + \hat{V} \frac{\partial D}{\partial \eta} \right) - \\ \left[ (1 + \sigma) \frac{\partial \zeta}{\partial t} + \hat{U} \frac{\partial \zeta}{\partial \xi} + \hat{V} \frac{\partial \zeta}{\partial \eta} \right] \end{aligned} \quad (28)$$

### Boundary and Initial Conditions

Eqs. (23)–(28) and Eq. (6) are solved prognostically as initial value problems of oceanic motion. The initial condition of the velocity takes  $u_1 = v_1 = 0$ . The boundary conditions are specified based on the oceanic problems we will study. For example, for closed basins like the Great Lakes, the boundary condition is specified as  $v_n = 0$  where  $v_n$  is the normal velocity component at the boundary. In the semi-enclosed basin or continental shelf, the sea-surface elevation (amplitude and phase of tidal forcing) is specified at the open boundary. The surface boundary conditions include (1) wind stress, (2) net surface heat flux and (3) precipitation/evaporation. Time variable river/dam and onshore intake/outfall discharges also are included as lateral boundary conditions in the model for the study of the buoyancy-driven circulation caused by river discharges.

### THE NUMERICAL COMPUTATIONAL METHOD

Eqs. (22)–(27) are very similar to the primitive equations in the curvilinear orthogonal and  $\sigma$ -coordinate systems used in the POM or ECOM-si except for extra terms related to  $h_3$ ,  $\hat{U}$  and  $\hat{V}$ . This non-orthogonal coordinate transformation model is identical to the ECOM-si as  $h_3 = 0$ , and  $J = h_1h_2$  in an orthogonal case. The numerical methods used for solving the ECOM-si are directly adopted to this non-orthogonal coordinate transformation model with some modifications. To provide more accurate water, heat and salt transports, the nonlinear advection terms in momentum, temperature, and salinity equations of the non-orthogonal coordinate model are calculated using the multidimensional positive definite advection transport algorithm (Smolarkiewicz 1984, Smolarkiewicz and Clark 1986). A semi-implicit scheme is used for the time integration (Casulli 1990), in which the free surface gradients in the momentum equations and transport terms in the continuity equations are treated implicitly. In the original code of the ECOM-si, the solution for the free surface elevation is achieved by solving a linear, symmetric, 5-diagonal matrix sys-

tem. In the non-orthogonal coordinate transformation model, however, the extra terms in the momentum equations result in a 9-diagonal matrix system that cannot be solved efficiently by preconditioned conjugate gradient methods. For this reason, we treat all terms related to  $h_3$  using the values in the previous time step, then the equations used to calculate the free surface elevation become a positive definite, symmetric, and 5-diagonal system as the same as the ECOM-si (Blumberg and Mellor 1987). After this treatment, the non-orthogonal coordinate transformation model can be solved numerically using the same semi-implicit approach used in the ECOM-si. Vertical diffusion terms in both momentum and temperature/salinity equations also are computed implicitly. When the advections and horizontal/vertical diffusions vanish in the momentum balance, the Euler forward scheme used in the ECOM-si becomes numerically unstable (Mesinger and Arakawa 1976). A predicted-corrector scheme (Wang and Ikeda 1995) is adopted to compute the Coriolis terms in the momentum equations.

An Arakawa C-grid is used in the numerical integration (Arakawa 1966). The grid generation program is developed by modifying Winslow's method for the automatic generation of computational meshes (Winslow 1966, Brackbill and Saltzman 1982). Winslow's method requires us to solve a nonlinear Poisson equation for generating a grid mapping from a regular numerical domain to an irregular-shape physical domain. This method is extended to adaptive mesh with varying zone sizes and orthogonality of grid lines (Brackbill and Saltzman 1982). We adopt this method to create orthogonal grids off the coast or near the open boundaries. We then employ our own "Matlab" program to modify grids near the coast to assume the shape of quadrilaterals for fitting the coastlines. This approach helps us avoid numerical instability problems that may occur due to improper treatment of open boundary conditions in the non-orthogonal coordinate transformation model.

### THE MODEL APPLICATION AND VALIDATION

To test our new non-orthogonal coordinate transformation oceanic circulation model, we applied it to Lake Superior for the study of coastal thermal front and a near-shore current jet (Fig. 1). In the western shore of Lake Superior's Keweenaw Peninsula, the coastal current is characterized by a strong coastal jet known as the Keweenaw Current (Har-

rington 1895, Hooper *et al.* 1973). The formation of this current is due to an intense temperature front over steep bottom topography near the shore and an onshore Ekman transport caused by westerly or southwesterly winds (Smith and Ragotzkie 1970, Chen *et al.* 2001, and Zhu *et al.* 2001). Because the cross-shelf scale of the thermal front and current jet is less than 10 km over a sharp decrease of the bottom topography, a proper fitting of the coastline and bottom topographies becomes essential for a successful simulation of the Keweenaw Current. In our model experiments, the irregular bathymetry is fitted by the  $\sigma$ -transformation coordinate system in the vertical. Under sufficient horizontal resolution, this transformation can accurately resolve the dynamics related to the steep bottom topography. The non-orthogonal coordinate transformation in the horizontal provides an accurate matching of the irregular coastline, which avoids a velocity error due to an improper solid boundary condition.

To validate our non-orthogonal grid Lake Superior model, we compared the simulation results of the near shore Keweenaw Current in southern Lake Superior obtained from curvilinear orthogonal and non-orthogonal transformation models. The validation of these two models was based on the agreement with observations. The model domain for both orthogonal and non-orthogonal cases is shown in Figure 3, which covers the entire lake with a high resolution of grids near the Keweenaw coast. The horizontal model grid cells were 123 (along-shelf)  $\times$  126 (cross-shelf). Horizontal resolution was about 300 to 600 m in the cross-shelf direction and 4 to 6 km in the along-shelf direction off the Keweenaw coast. The model grid cells were orthogonal in the interior of the lake for both cases. In the non-orthogonal case, the quadrilaterals were used to fit the irregular shape of the coastline (Fig. 4a), while in the orthogonal case, the coastline was treated as a smoothed curvature line as shown in Figure 4b. To satisfy the restriction of the exact orthogonal requirement, the boundary cells in the orthogonal case reduced a certain level of the resolution as that shown in the non-orthogonal case. In both the orthogonal and non-orthogonal cases, the 31 uniform  $\sigma$ -levels are used in the vertical, which resulted in a vertical resolution of about 1 m near the coast and 10 m at the 300-m isobath in the interior of the lake. The time step was 360 seconds.

The model was forced by observed winds and heat flux taken in July 1973 near Eagle Harbor. The surface wind stress was calculated using Large and Pond's formula with a neutral, steady-state drag

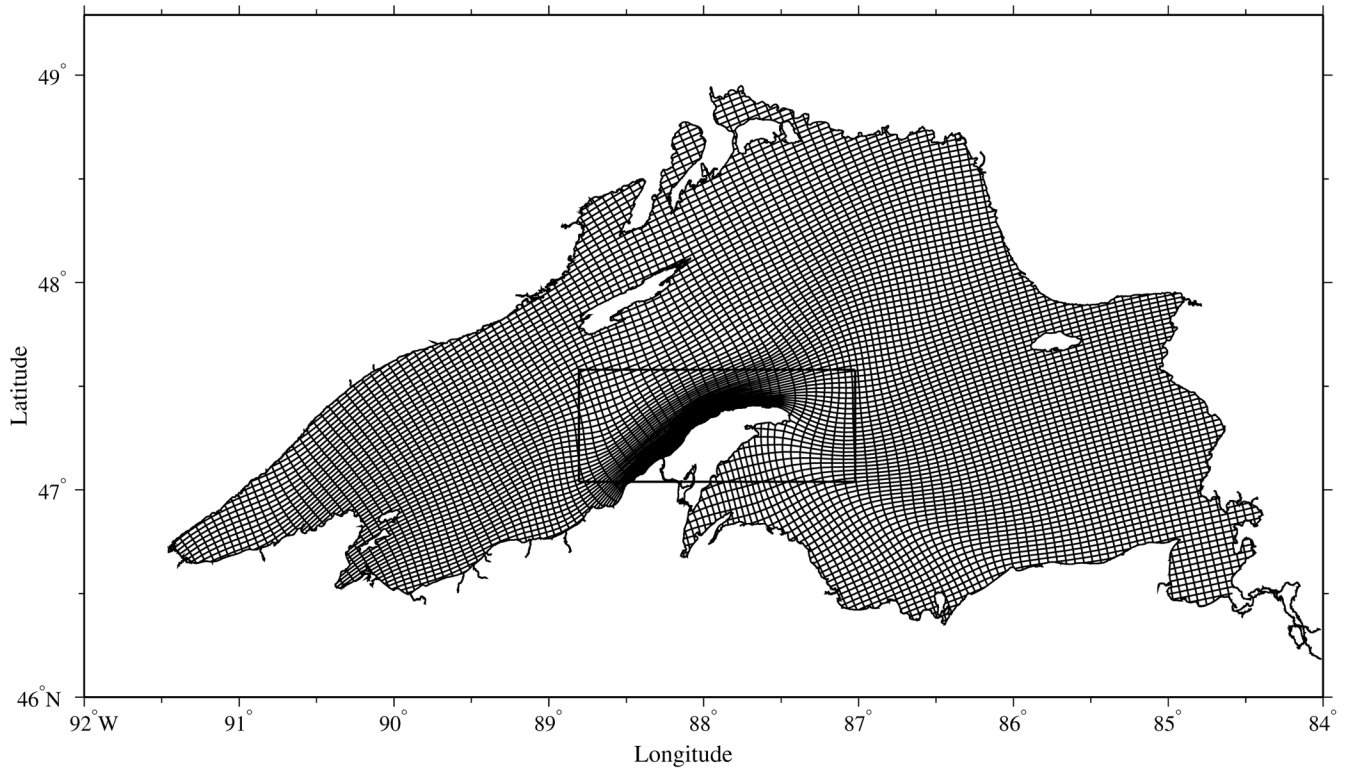


**FIG. 3.** *Non-orthogonal coordinate transformation model grids for Lake Superior.*

coefficient (Large and Pond 1981). The heat flux data included both net surface heat flux and short-wave radiation. The initial stratification was set up using observed temperature data taken regionally over the lake in early July. Surface temperature was about 14°C at the coast and decreased to 5°C over a cross-shelf distance of 5 km. The large vertical temperature gradient only existed in the upper 60 m.

Figure 5 shows the comparisons between model-predicted and observed current speed at the near-surface at buoy stations 1–3 (see Fig. 2 for the locations of these three buoys). The current data used for this comparison was provided by Joe Niebauer at the University of Wisconsin-Madison (Niebauer *et al.* 1977). The observational data were taken in July of 1973. Buoys 1 and 2 were deployed about 0.7 km and 2.5 km off the coast near Eagle Harbor. The model-predicted currents calculated using the non-orthogonal coordinate transformation model were in good agreement with observed currents at all three buoy stations, while the orthogonal coordinate transformation model significantly underestimated the magnitude of the current at near-shore buoy stations 1 and 2. Because the original orthogonal and newly developed non-orthogonal versions

of the model have the exact same physics, the difference found in these two cases is due to the accuracy of the coastline fitting. This also explains why no numerical simulations could successfully simulate the Keweenaw Current in Lake Superior until our efforts using this new non-orthogonal coordinate transformation model.

The new non-orthogonal coordinate transport model introduced here also provided a reasonable simulation of the thermal front and Keweenaw Current measured during the KITES field programs. For example, the satellite-derived SST showed a narrow thermal front on 17 September 1999 (Fig. 6: upper-left). This front was reasonably captured by the model simulation (Fig. 6: lower-left). The ADCP data received at site E3 showed two strong along-shore currents during 9–11 September and 13–15 September, respectively. The currents weakened with depth, having a vertical scale of about 60 and a speed of 60 cm/s at a depth of 17 m (Fig. 6: upper-right). These along-shore currents were captured up reasonably by the model (Fig. 6: lower-right). These comparisons suggest that this model is a robust tool for the study of the near-shore physical process in Lake Superior.

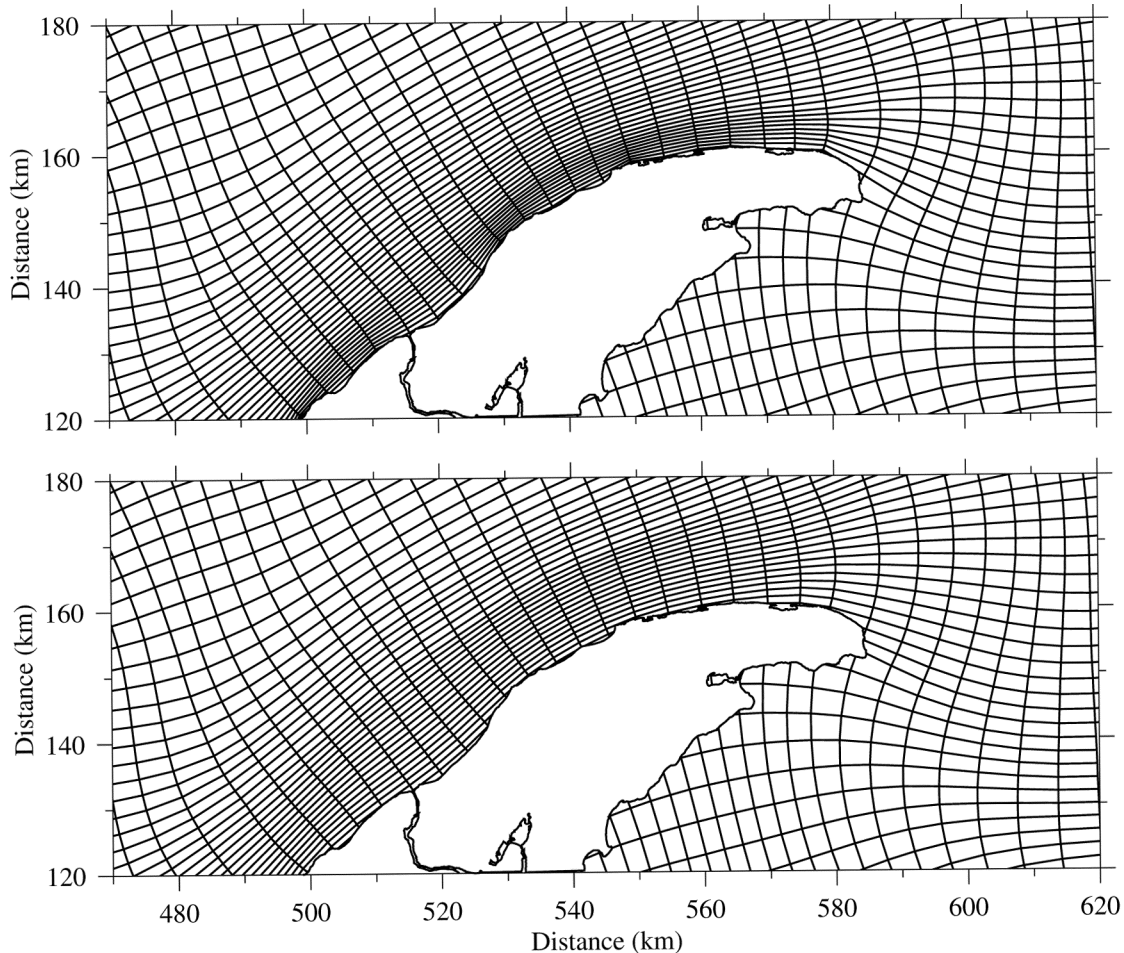


**FIG. 4.** Numerical grids along the Keweenaw coast for the non-orthogonal coordinate transformation (upper panel) and orthogonal coordinate transformation (lower panel).

### CONCLUSION

A non-orthogonal coordinate primitive equation model has been developed for the study of the inner-shelf coastal oceanic circulation. A version of the non-orthogonal coordinate transformation used in this model provides a more accurate fitting of the coastline, which allows us to simulate the near-coastal physical processes such as tides, coastal fronts, and current jet. By removing the requirement of a strict orthogonal condition, this model provides an easier and faster convergence for grid generation. The model is computed numerically using a finite difference method. The numerical program of the model has been written based on the semi-implicit code of Blumberg and Mellor's curvilinear orthogonal coastal ocean circulation model (ECOM-si) with some modifications to allow for

inclusion of non-orthogonal transformation terms and correction of the calculation of the Coriolis terms. Therefore, users who are familiar with POM or ECOM-si can easily learn how to use this model.

The numerical program of this non-orthogonal grid model was tested first by running it parallel with ECOM-si under orthogonal grids for the study of the formation of the thermal front and current jet along the Keweenaw coast. Given the same horizontal resolution, the comparison between the model-predicted currents obtained by the model runs with orthogonal and non-orthogonal coordinate transformations shows that the non-orthogonal grid model provided much more accurate simulation for the near-shore current jet observed along the Keweenaw coast in Lake Superior. Also, this newly-developed non-orthogonal model has suc-

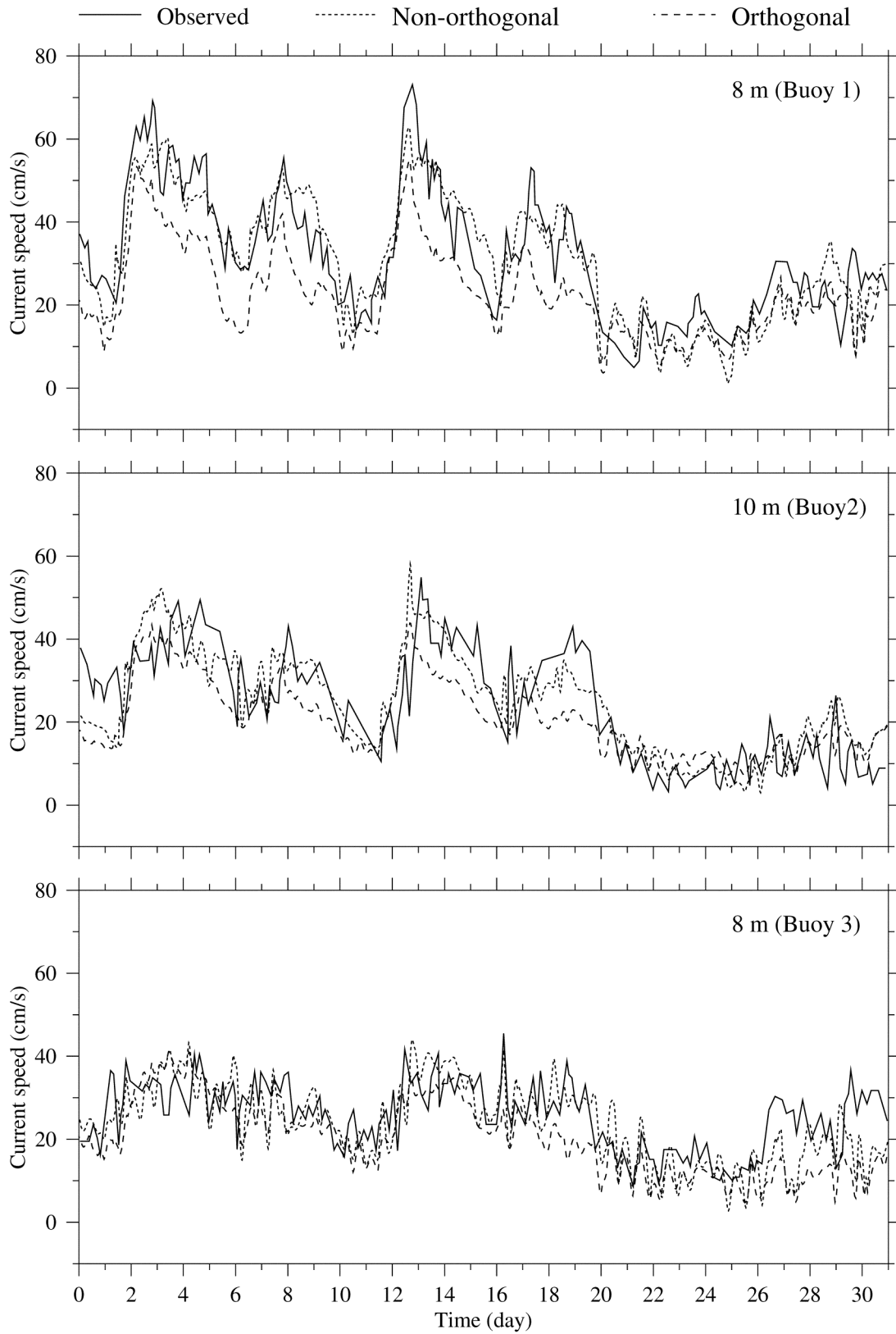


**FIG. 5.** Time series of observed (solid line) and model-predicted current speeds at the surface of 8 or 10 m at buoys 1, 2, and 3 for July of 1973.

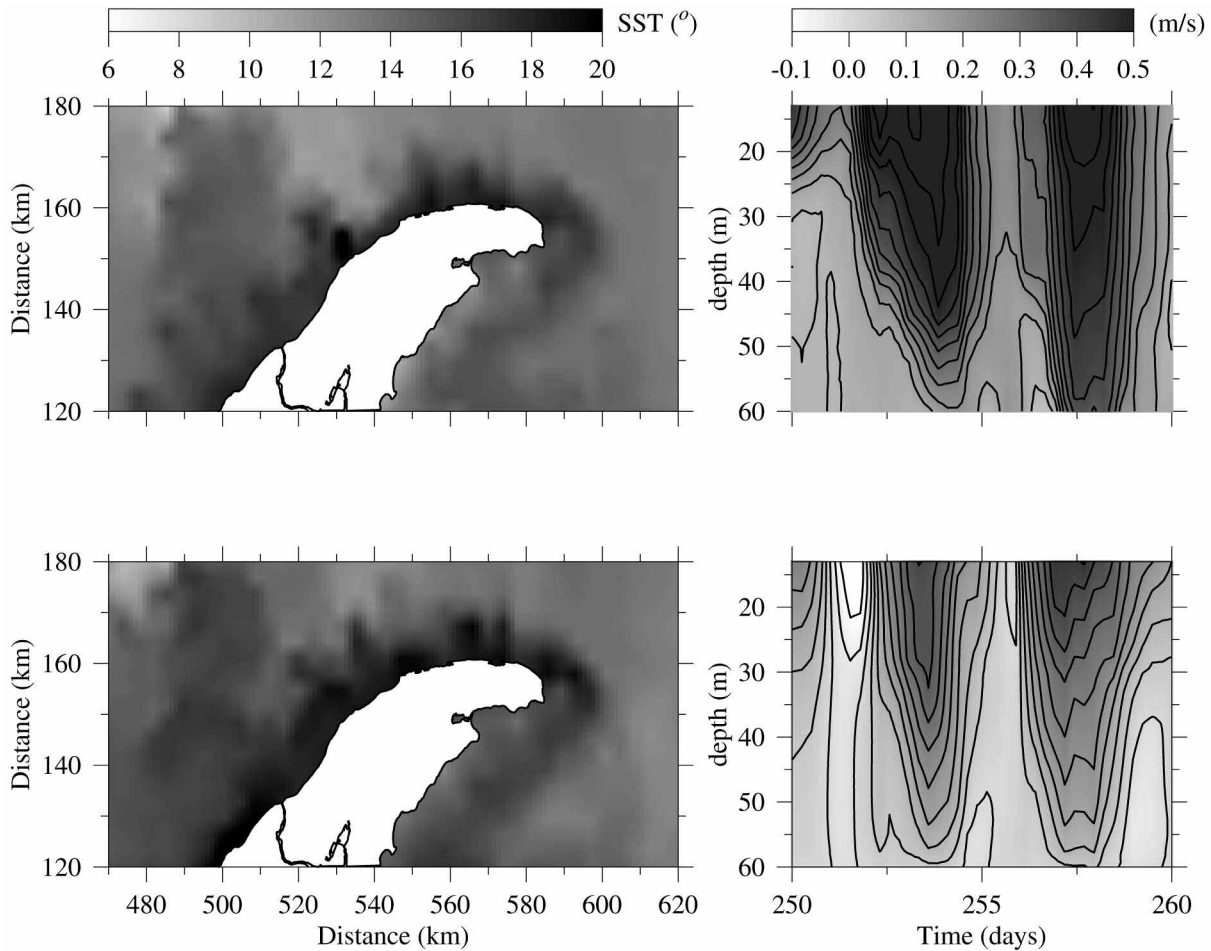


**FIG. 6.** Comparison between the satellite-derived and model-computed SST and along-shore currents. Left: the satellite-derived (upper) and model-predicted (lower) SST distribution along the Keweenaw coast on 17 September, 1999. Right: the ADCP measured (upper) and model-computed (lower) vertical profiles of the along-shore current at site E3 during 11–15 September 1999.

cessfully captured the spatial structure of the thermal current and Keweenaw Current measured during the 1999 KITES field measurement. This study has provided us with a good example of the validation of this non-orthogonal model to the study of the near-shore current system.

#### ACKNOWLEDGMENTS

This research was supported by the National Science Foundation under grant number OCE-9712869 and 0196543. We want to thank Joe Niebauer for sending us figures of observed currents taken near the Eagle Harbor in July of 1973 and for giving us permission to use his data for the model-data comparison. We also thank George Davidson at Univer-

sity of Georgia for his editorial help on this manuscript.

#### APPENDIX

The non-orthogonal coordinate transformation introduced in our paper is different from the non-orthogonal coordinate model introduced in CH3D or CH3D-WES. In our model,  $u_1$  and  $v_1$  are defined as the  $e_\xi$  and  $e_\eta$  components of the velocity vector (see Fig. 1), where  $e_\xi$  and  $e_\eta$  are the unit vectors tangent to curves  $\xi$  and  $\eta$  defined as

$$e_\xi = \frac{\xi_x \cdot i + \xi_y \cdot j}{\sqrt{\xi_x^2 + \xi_y^2}}, \quad e_\eta = \frac{\eta_x \cdot i + \eta_y \cdot j}{\sqrt{\eta_x^2 + \eta_y^2}}, \quad (\text{A1})$$

where  $\xi = \xi(x, y)$ ,  $\eta = \eta(x, y)$ ,  $\xi_x = \frac{y_\eta}{J}$ ,  $\xi_y = -\frac{x_\eta}{J}$ ,  
 $\eta_x = -\frac{y_\xi}{J}$ ,  $\eta_y = \frac{x_\xi}{J}$ , and  $J = x_\xi \cdot y_\eta - x_\eta \cdot y_\xi$ .

Substituting  $\xi_x$ ,  $\xi_y$ ,  $\eta_x$ ,  $\eta_y$  into  $e_\xi$  and  $e_\eta$  yields

$$e_\xi = \frac{1}{h_2} (y_\eta \cdot i - x_\eta \cdot j), \quad e_\eta = \frac{1}{h_1} (-y_\xi \cdot i + x_\xi \cdot j) \quad (\text{A2})$$

where

$$h_1 = \sqrt{x_\xi^2 + y_\xi^2}, \quad h_2 = \sqrt{x_\eta^2 + y_\eta^2}.$$

By this definition, we can get a relationship between  $(u_1, v_1)$  and  $(u, v)$  (the x and y components of the horizontal velocity on the orthogonal coordinate) as

$$\begin{cases} u_1 = \frac{h_2}{J} (x_\xi u + y_\xi v) \\ v_1 = \frac{h_1}{J} (x_\eta u + y_\eta v) \end{cases} \quad (\text{A3})$$

This definition provides simple expressions of the momentum and tracer equations like those shown in an orthogonal coordinate model.

In CH3D or CH3D-WES,  $u_1$  and  $v_1$  are defined as

$$u_1 = \frac{d\xi}{dt} \quad \text{and} \quad v_1 = \frac{d\eta}{dt}. \quad (\text{A4})$$

By this definition,  $(u_1, v_1)$  has a relationship with  $(u, v)$  as follows:

$$\begin{cases} u_1 = \frac{1}{J} (y_\eta u - x_\eta v) \\ v_1 = \frac{1}{J} (-y_\xi u + x_\xi v) \end{cases} \quad (\text{A5})$$

Let us define  $(e_{\xi 2}, e_{\eta 2})$  as the direction vectors of  $u_1$  and  $v_1$  in the non-orthogonal coordinates introduced in CH3D, and then

$$u = x_\xi u_1 + x_\eta v_1, \quad v = y_\xi u_1 + y_\eta v_1. \quad (\text{A6})$$

According to the definition of a vector:

$$V = u \cdot i + v \cdot j = u_1 e_{\xi 2} + v_1 e_{\eta 2}, \quad \text{i.e.,}$$

$$J(ui + vj) = (y_\eta e_{\xi 2} - y_\xi e_{\eta 2})u + (-x_\eta e_{\xi 2} + x_\xi e_{\eta 2})v, \quad (\text{A7})$$

so that

$$\begin{cases} i = \frac{1}{J} (y_\eta e_{\eta 2} - y_\xi e_{\xi 2}) \\ j = \frac{1}{J} (-x_\eta e_{\xi 2} + x_\xi e_{\eta 2}) \end{cases}, \quad (\text{A8})$$

and

$$\begin{cases} e_{\xi 2} = (x_\xi i + y_\xi j) \\ e_{\eta 2} = (x_\eta i + y_\eta j) \end{cases}; \quad \begin{cases} |e_{\xi 2}| = \sqrt{x_\xi^2 + y_\xi^2} = h_1 \\ |e_{\eta 2}| = \sqrt{x_\eta^2 + y_\eta^2} = h_2 \end{cases}. \quad (\text{A9})$$

Therefore,  $e_{\xi 2}$  and  $e_{\eta 2}$  are not the unit vectors! Because

$$\begin{aligned} e_\xi \cdot e_{\eta 2} &= \frac{1}{h_2} (y_\eta i - x_\eta j) \cdot (x_\eta i + y_\eta j) = 0 \\ e_\eta \cdot e_{\xi 2} &= \frac{1}{h_2} (-y_\xi i + x_\xi j) \cdot (x_\xi i + y_\xi j) = 0 \end{aligned}$$

$e_{\xi 2}$  and  $e_{\eta 2}$  are in the directions normal to  $e_\eta$  and  $e_\xi$  respectively (see Fig. 7).

In the non-orthogonal coordinate defined in CH3D and CH3D-WES, all the force terms like pressure gradient forces, Coriolis forces, etc., are divided into two terms in each component. This makes that model structure much more complicated than those in the orthogonal coordinate system and

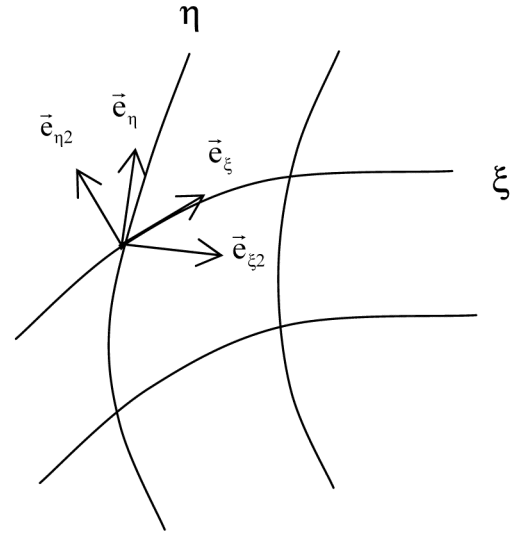


**FIG. 7. Illustration of the non-orthogonal coordinate system used in CH3D or CH3D-WES and the relationship between  $(e_{\xi 2}$  and  $e_{\eta 2})$  in CH3D and  $(e_\xi$  and  $e_\eta)$  in our model..**

in the non-orthogonal coordinate introduced in this paper. In addition, when the sigma-coordinate transformation is used in a stratified fluid, it leads to numerical errors on sloping bottom topography due to the inaccurate computation of the baroclinic pressure gradient force (Haney 1991, Chen and Beardsley 1995). Dividing the pressure gradient terms into two terms in each momentum equation probably would make it more difficult to minimize the sigma-coordinate error.

## REFERENCES

- Arakawa, A. 1966. Computational design for long-term numerical integration of the equation of fluid motion: two dimensional incompressible flow. *J. Comput. Phys.* 1:119–143.
- Bennett, E.B. 1978. Characteristics of the thermal regime of Lake Superior. *J. Great Lakes Res.* 4:310–319.
- Blumberg, A.F. 1994. *A Primer for ECOM-si*. Technical Report of HydroQual, Inc.
- , and Mellor, G.L. 1987. A description of a three-dimensional coastal ocean circulation model. In *Three-dimensional coastal models*, ed. N.S. Heaps, pp. 1–16. Coastal Estuarine Science.
- Brackbill, J.U., and Saltzman, J.S. 1982. Adaptive zoning for singular problems in two dimensions. *J. Comput. Phys.* 46:342–368.
- Casulli, V. 1990. Semi-implicit finite-difference methods for the two-dimensional shallow water equations. *J. Comput. Phys.* 86:56–74.
- Chapman, R.S., Johnson, B.H., and Vemulakonda, S.R. 1996. *A three-dimensional numerical hydrodynamic, salinity, and temperature model*. U.S. Army Corps of Engineers, Waterways Experiment Station Technical Report HL-96-21.
- Chen, C., and Beardsley, R.C. 1995. Numerical study of stratified tidal rectification over finite-amplitude banks. Part I: symmetric banks. *J. Phys. Oceanogr.* 25:2090–2110.
- , Zhu, J., Ralph, E., Green, S.A., and Budd, J. 2001. Prognostic modeling studies of the Keweenaw current in Lake Superior. Part I: formation and evolution. *J. Phys. Oceanogr.* 31:379–395.
- Galperin, B., Kantha, L.H., Hassid, S., and Rosati, A. 1988. A quasi-equilibrium turbulent energy model for geophysical flows. *J. Atmos. Sci.* 45:55–62.
- Haney, R.L. 1991. On the pressure gradient force over steep topography in sigma coordinate ocean models. *J. Phys. Oceanogr.* 21:610–619.
- Harrington, M.W. 1895. *Surface current of the Great Lakes*. U.S. Department of Agriculture, Weather Bureau Bull.
- Hooper, J.A., Ragotzkie, R.A., Lien, S.L., and Smith, N. P. 1973. *Circulation patterns in Lake Superior*. Tech. Rep. Wis WRC 73-04, Water Resources Center, Univ. of Wisconsin, Madison, Wisconsin.
- Hubbard, D.W., and Spain, J.D. 1973. The structure of the early spring thermal bar in Lake Superior. In *Proc. 16th Conf. Great Lakes Res.*, pp. 735–742. Internat. Assoc. Great Lakes Res.
- Jacobs, S.J. 1974. On wind-driven lake circulation. *J. Phys. Oceanogr.* 4:392–399.
- Lam, D.C. 1978. Simulation of water circulation and chloride transports in Lake Superior for summer 1973. *J. Great Lakes Res.* 4:343–349.
- Large, W.S., and Pond, S. 1981. Open ocean momentum flux measurements in moderate to strong winds. *J. Phys. Oceanogr.* 11:324–406.
- Mellor, G.L., and Yamada, T. 1974. A hierarchy of turbulence closure models for planetary boundary layers. *J. Atmos. Sci.* 31:1791–1806.
- , and Yamada, T. 1982. Development of a turbulence closure model for geophysical fluid problems. *Rev. Geophys. Space. Phys.* 20:851–875.
- Mesinger, F., and Arakawa, A. 1976. *Numerical Methods Used in Atmospheric Models*. GARP Publication Series, 1, WMO-ICSU Joint Organizing Committee.
- Niebauer, H.J., Green, T., and Ragotzkie, R.A. 1977. Coastal upwelling/downwelling cycles in southern Lake Superior. *J. Phys. Oceanogr.* 7(6):918–927.
- Phillips, D.W. 1978. Environmental climatology of Lake Superior. *J. Great Lakes Res.* 4:288–309.
- Ragotzkie, R.A. 1966. *The Keweenaw Current, a regular feature of summer circulation of Lake Superior*. Tech. Rep. No. 29, Univ. Wisconsin.
- Sheng, Y.P. 1986. *A three-dimensional mathematical model of coastal, estuarine and lake currents using boundary fitted grid*. Report No. 585. A. R. A. P. Group of Titan Systems, New Jersey, Princeton, NJ.
- Smagorinsky, J. 1963. General circulation experiment with the primitive equations. I. The basic experiments. *Mon. Weather Rev.* 91:99–164.
- Smith, R.L., and Ragotzkie, R.A. 1970. A comparison of computed and measured currents in Lake Superior. In *Proc. 13th Conf. Great Lakes Res.*, pp. 969–977. Internat. Assoc. Great Lakes Res.
- Smolarkiewicz, P.K. 1984. A fully multidimensional positive definite advection transport algorithm with small implicit diffusion. *J. Comput. Phys.* 54:325–362.
- , and Clark, T.L. 1986. The multidimensional positive definite advection transport algorithm: further development and applications. *J. Comput. Phys.* 86:355–375.
- Spain, J.D., Wernet, G.M., and Hubbard, D.W. 1976. The structure of the spring thermal bar in Lake Superior, II. *J. Great Lakes Res.* 2:296–306.
- Viekman, B.E., and Wimbush, M. 1993. Observation of the vertical structure of the Keweenaw Current, Lake Superior. *J. Great Lakes Res.* 19:470–479.
- Wang, J., and Ikeda, M. 1995. Stability analysis of finite difference schemes for inertial oscillations in ocean general circulation model. In *Computer Modeling of*

- Seas and Coastal Regions*, ed. C.A. Brebbia *et al.*, pp. 19–27. Computational Mechanics Publications, Southampton.
- Winslow, A.M. 1966. Numerical solution of the quasilinear Poisson equation in a nonuniform triangle mesh. *J. Comput. Phys.* 1:149–172.
- Zhu, J., Chen, C., Ralph, E., Green, S.A., and Budd, J. 2001. Prognostic modeling studies of the Keweenaw Current in Lake Superior. Part II: simulation. *J. Phys. Oceanogr.* 31:396–410.
- Submitted: 8 May 2002*  
*Accepted: 7 May 2004*  
*Editorial handling: Martin T. Auer*